Aalborg Universitet

AALBORG UNIVERSITY
DENMARK

Sensorless State of Temperature Estimation for Smart Battery based on Electrochemical Impedance

Zheng, Yusheng; Weinreich, Nicolai André; Kulkarni, Abhijit; Che, Yunhong; Sorouri, Hoda; Sui, Xin; Teodorescu, Remus

Published in:
2023 25th European Conference on Power Electronics and Applications, EPE 2023 ECCE Europe

DOI (link to publication from Publisher):
10.23919/EPE23ECCEEurope58414.2023.10264452

Publication date:
2023

Document Version
Accepted author manuscript, peer reviewed version

Link to publication from Aalborg University

Citation for published version (APA):
Zheng, Y., Weinreich, N. A., Kulkarni, A., Che, Y., Sorouri, H., Sui, X., & Teodorescu, R. (2023). Sensorless State of Temperature Estimation for Smart Battery based on Electrochemical Impedance. In *2023 25th European Conference on Power Electronics and Applications, EPE 2023 ECCE Europe* (pp. 1-8). Article 10264452 IEEE. https://doi.org/10.23919/EPE23ECCEEurope58414.2023.10264452

General rights
Copyright and moral rights for the publications made accessible in the public portal are retained by the authors and/or other copyright owners and it is a condition of accessing publications that users recognise and abide by the legal requirements associated with these rights.

- Users may download and print one copy of any publication from the public portal for the purpose of private study or research.
- You may not further distribute the material or use it for any profit-making activity or commercial gain
- You may freely distribute the URL identifying the publication in the public portal -

Take down policy
If you believe that this document breaches copyright please contact us at vbn@aub.aau.dk providing details, and we will remove access to the work immediately and investigate your claim.

Sensorless State of Temperature Estimation for Smart Battery based on Electrochemical Impedance

Yusheng Zheng, Nicolai André Weinreich, Abhijit Kulkarni, Yunhong Che, Hoda Sorouri, Xin Sui, Remus Teodorescu
Department of Energy, Aalborg University
Aalborg, Denmark

Acknowledgments

This work was supported in part by the Villum Foundation for Smart Battery project (No. 222860).

Keywords

«Electric Vehicle (EV)», «Batteries», «Battery impedance measurement», «Battery Management Systems (BMS)», «Energy storage».

Abstract

Temperature plays a significant role in the safety, performance, and lifetime of lithium-ion batteries (LIBs). Therefore, monitoring battery temperature becomes one of the fundamental tasks for the safe and efficient operation of LIBs. Given the limited onboard temperature sensors, this paper proposes a sensorless temperature estimation method suitable for the smart battery system by obtaining the electrochemical impedance of batteries online via bypass actions. A suitable frequency is selected from the battery electrochemical impedance spectroscopy (EIS) to achieve an accurate and robust estimation of the battery temperature through online impedance measurement. Using the battery impedance with this selected frequency, the battery temperature can be estimated under different scenarios, with RMSE less than 1.5 ℃.

Introduction

Owing to the superiority in energy and power density, charge and discharge efficiency, as well as cycle life, LIBs are being widely applied in many energy storage systems. The large-scale applications of LIBs in electric mobilities such as electric vehicles (EVs), electric aircraft, and stationary battery energy storage systems of smart grids, have received increasing attention over the years. For instance, the global EV sales for 2022 exceeded 10.5 million, with a significant increase of 55% compared to that in 2021 [1]. With the wide adoption of LIBs in renewable energy storage systems, the safety, performance, and durability of the battery system become the main concern. The battery management system (BMS) plays an essential role in the battery system by monitoring the key states of LIBs, such as the state of charge (SOC) and state of temperature (SOT), and balancing cells in order to guarantee safe and efficient operations of the battery system [2].

The temperature has a great impact on the safety, performance, and degradation of LIBs [3]. Specifically, extremely high temperatures increase the risk of thermal runaway, which might cause catastrophic consequences [4]. Extreme low temperatures, on the other hand, undermine the energy and power capability of LIBs by causing sluggish electrochemistry inside the cell [4]. Furthermore, both high and low temperatures can cause accelerated battery aging, which greatly reduces the lifetime of batteries [5]. Therefore, the temperature of each battery cell inside the pack needs to be properly monitored and regulated in order to ensure the safety and high performance of the battery system. Nevertheless, in real-world applications, the number of temperature sensors in a battery pack is very limited due to cost constraints. According to ref. [6], the average sensor-to-cell ratio in a battery pack of EVs is close to 1/10. In this regard, there is an urgent need to develop sensorless temperature estimation methods by taking advantage of other measured signals such as current and voltage.

There are several ways to achieve sensorless temperature estimation. Among them, electrochemical impedance-based estimation exhibit advantages in simplicity and easy implementation thanks to the development of online electrochemical impedance measurement [7]. Since electrochemical impedance is an indicator of the cell's internal electrochemistry, the change in the internal reactions caused by battery temperature change can also be reflected by the electrochemical impedance [8]. In this way, by measuring the impedance periodically, the battery temperature can be inferred. With the smart battery (SB) architecture [9], as shown in

Fig. 1, the online measurement of the impedance can be easily achieved. Such an architecture is comprised of a half-bridge circuit with MOSFETs connected to each cell. A slave CPU is used to control the switches in order to decide whether to bypass the cell or not [9]. With controlled bypass actions, pseudo-random sequences with different frequency ranges can be generated to obtain battery impedance online. Afterward, battery temperature can be estimated based on such online impedance measurements.

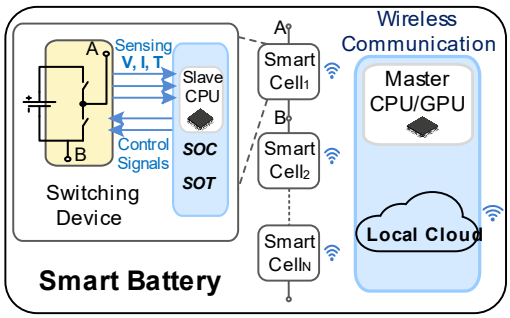

Fig. 1: The architecture of the smart battery management system [9].

Nevertheless, measuring the battery electrochemical impedance in a wide frequency range (e.g., from 0.01Hz - 10kHz) is time-consuming, making it impossible for the BMS to monitor battery SOT timely. Hence, the electrochemical impedance of LIBs can only be measured at certain frequencies to meet the demand of real-time estimation. To date, there is still no quantitative analysis in the literature regarding the selection of the excitation frequencies for SOT estimation. Toward this end, this paper proposes a methodology for sensorless SOT estimation by selecting a suitable frequency for electrochemical impedance measurement. Particularly, the EIS of LIBs is measured under different SOCs and temperatures. The change in the battery impedance with SOCs and temperatures is analyzed. Then the frequency under which impedance parameters are sensitive to temperature change is selected based on the EIS analysis. Finally, the estimation performance using the impedance parameter at this frequency is verified under different temperatures.

In the following, the online impedance measurement in smart batteries will be introduced first. Then the impedance measurement in smart batteries and the proposed methodology for online temperature estimation are presented, followed by the experiments for EIS measurement and results of estimation.

Impedance measurement in smart batteries

The SB architecture shown in Fig. 1 consists of a half-bridge topology integrated into each cell. The switching of the half-bridge is driven by the slave CPU. Consider the case when the cells in an SB pack are under constant current (CC) charging. By pulsating the half-bridge switches, the current into any cell can be adjusted to any desired frequency. Thus, the SB architecture enables the online measurement of battery impedance at any desired frequency, as shown in Fig. 2.

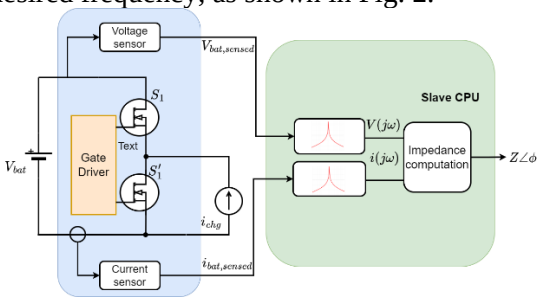

Fig. 2: Online impedance measurement in the slave processor of an SB cell [10].

As can be seen from Fig. 2, the half-bridge switches are controlled to produce a square wave current into the cell. This is because when the top device S_1 is ON, the cell takes the charging current while the current through the cell is zero when S_1' is ON. The cell current and voltages can be measured online by SB as highlighted in Fig. 1. These sensed voltages and currents are processed with a narrow bandpass filter to extract the desired frequency components. The impedance can be expressed by the transfer function as,

$$Z(j\omega) = \frac{V(j\omega)}{I(j\omega)} = |Z|\angle\phi \qquad (1)$$

where $|Z|$ is the magnitude of the transfer function and ϕ is the phase.

The impedance thus computed is connected with the sensorless temperature estimation methodology described next.

Methodology

The key idea of sensorless SOT estimation is to take advantage of the temperature dependency of battery impedance to estimate battery temperature according to the online impedance measurements. Typically, the EIS of the battery is measured by sweeping the frequency of the excitation current over a wide range from 0.01 Hz to 10 kHz and calculating the corresponding impedance, which usually takes at least half an hour. In real applications, however, it is impractical to

measure the battery EIS over such a wide frequency range. Otherwise, the battery SOT cannot be obtained timely. Therefore, only the impedance at some specific frequencies can be measured online for SOT estimation.

In this paper, we propose an online SOT estimation method by selecting an appropriate excitation frequency. Under this frequency, the battery impedance must be sensitive to the temperature change. By measuring the battery impedance at this frequency in real-time, the SOT can be also estimated timely based on the measurement. However, the battery impedance Z is not only dependent on the excitation frequency f and temperature T, but also on the SOC, which can be expressed as,

$$Z = g(f, T, SOC) \quad (2)$$

The dependency of the impedance on multiple factors makes it difficult to estimate SOT accurately since other factors might interfere with the estimation process. To eliminate the influence of other factors such as SOC on estimation, a suitable frequency f^* can be found under which the impedance of the battery changes notably with the battery temperature but remains constant at different SOC. In order to obtain the sensitivity of the impedance to different factors, the impedance-temperature relationship can be approximated by fixing the frequency and SOC and performing the linear regression,

$$Z = \alpha_1 T + \beta_1 \quad (3)$$

The impedance sensitivity to temperature is then estimated by $\alpha_1 = \mathrm{d}Z/\mathrm{d}T$. Similarly, the impedance-SOC relationship can be approximated as,

$$Z = \alpha_2 SOC + \beta_2 \quad (4)$$

and the impedance sensitivity to SOC can be estimated as $\alpha_2 = \mathrm{d}Z/\mathrm{d}T$.

The frequency f^* is then the frequency where $|\mathrm{d}Z/\mathrm{d}T|$ is large and $|\mathrm{d}Z/\mathrm{d}SOC|$ is negligible, making the impedance sensitive to temperature change and independent of SOC and thus leading to a better condition for temperature estimation.

In this way, the battery impedance under f^* can be expressed as,

$$Z^* = g(T)|_{f=f^*} \quad (5)$$

And battery temperature can be estimated by performing the inverse function of (5) as,

$$\hat{T} = g^{-1}(Z^*) \quad (6)$$

Experimental setup

In this paper, a 3.7V/50Ah NMC LIB from CALB is used to conduct the EIS tests.

The experimental setup used in this study is illustrated in Fig. 3. In this setup, a Digatron battery tester, a thermal chamber, an electrochemical workstation, a temperature acquisition module, and a host computer are involved. The tested battery cell is placed in the thermal chamber where the ambient temperature can be adjusted and maintained around the test temperature. The test cell is also electrically connected to both the battery tester and electrochemical workstation. A K-type thermocouple is placed at the center of the battery cell to monitor the cell temperature during tests. The host computer, with the programmed test procedure, can control the battery tester and the electrochemical workstation during the test. The measured current, voltage, temperature, and battery EIS are stored in the host computer.

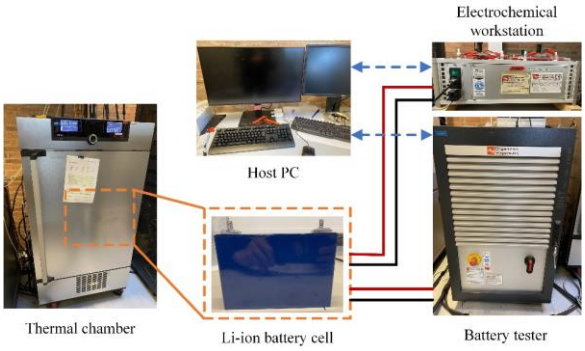

Fig. 3: Experimental setup for battery EIS tests.

The EIS of the battery cell is measured at different temperatures and SOCs, as summarized in Table I. At each tested temperature, the battery is fully charged at first using 1C constant current-constant voltage (CC-CV) protocol and then rested for 1 h. Afterward, the SOC is adjusted to the test SOCs using 50-A discharge current. The battery will rest for 1h after each SOC adjustment to reach the equilibrium state, followed by the EIS test. The frequency in the EIS test ranges from 0.01 Hz to 6400 Hz.

Table I: Summary of the EIS tests

Test temperatures	**Test SOCs**
15 ℃, 20 ℃, 25 ℃, 30 ℃, 35 ℃, 40 ℃, 45 ℃	90%, 70%, 50%, 30%, 10%

Results and discussion

In this section, the EIS test results will be presented and analyzed first. In this regard, according to the SB designed in Section II, the voltage and current in the SB are sensed when a narrowband filter extracts the desired frequency

component. Afterward, the SOT estimation will be conducted under two operating scenarios. In the first scenario, the battery SOC is kept at 50%, which is close to the operation of HEV where the battery pack is only used as an energy buffer and will not undergo significant SOC variation. In the second scenario, the battery SOT is estimated by considering different SOCs, since in battery electric vehicles (BEVs) and plug-in hybrid electric vehicles (PHEVs) the battery pack serves as the primary energy source so that the SOC will vary notably during charge and discharge cycles.

Experimental results

The impedance magnitude obtained from the filter's output in SB is compared with EIS test results. Fig. 4 compares the magnitudes of the impedances estimated by SB with those obtained from the EIS test results at different frequencies at 25 ℃ when the SOC is 50%. SB's average and maximum errors compared to the EIS test are 2.3% and 5.8%, respectively. A 2RC model obtains these values, and the error will be reduced by applying it to a real battery. The details of this model can be referred to [10].

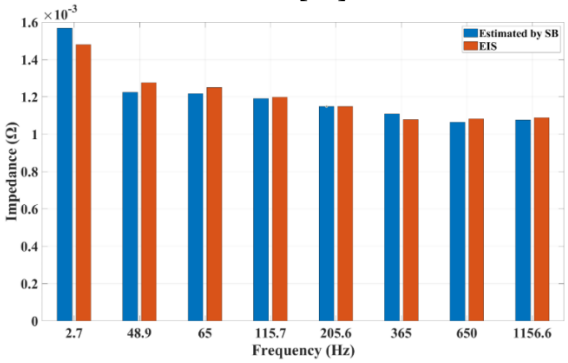

Fig. 4: Comparison between SB and EIS test.

Since the battery EIS varies with the temperature and SOC, the experimental results will be presented to illustrate how temperature and SOC influence battery EIS. First, to examine the effect of temperature on EIS, the battery SOC is kept at 50% and the result is illustrated in Fig. 5(a). At the high-frequency region, the imaginary part of the EIS becomes dominant with the increase of excitation frequency, and such inductance is affected by the wiring patterns rather than the property of the battery. Therefore, in this paper, the battery EIS under the frequency from 0.01 Hz to 1156 Hz is selected for illustration and further analysis. Furthermore, in Fig. 5(a), the EIS of the battery in the Nyquist plot shrinks towards the left side with the temperature increase, indicating a decrease in battery impedance. The change in battery EIS is more significant in the lower temperature range (i.e., 15-30 ℃) than that in the higher temperature range (i.e., 30-45 ℃).

To illustrate the change in battery EIS with SOC, the EIS at 25 ℃ under different SOCs is shown in Fig. 5(b). When SOC is higher than 30%, the battery EIS changes very slightly with SOC. In particular, the impedance at higher frequencies is virtually the same at different SOCs. At the low-frequency range, the EIS gradually diverges a little bit. Nevertheless, when SOC is lower than 30%, the EIS at the low-frequency region shifts remarkably towards the right side of the Nyquist plot, indicating significantly increased impedance.

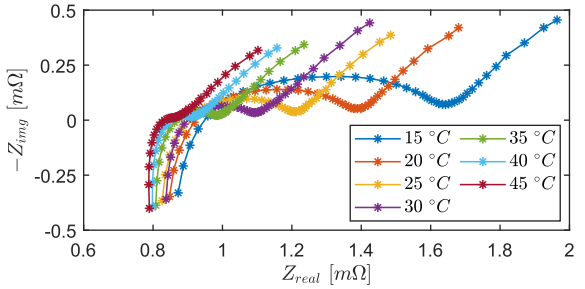

(a)

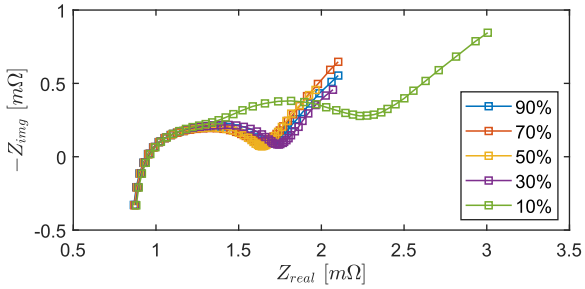

(b)

Fig. 5: Results of EIS tests at different temperatures and SOCs. (a) The EIS results at different temperatures when battery SOC is 50%, (b) The EIS results at different SOCs with battery temperature at 25 ℃.

It can be concluded from Fig. 5 that in a wide SOC region (i.e., 30% - 90%), the temperature has a more significant impact on the EIS than SOC does.

SOT estimation at 50% SOC

In the first scenario, the battery SOT will be estimated when the SOC is kept at 50%. To investigate how temperature changes the impedance parameters such as the real part, imaginary part, magnitude, and phase, the value of these parameters is extracted from the EIS and presented in the Bode plot in Fig. 6. The battery impedance can be expressed as follows,

$$Z = Z_{real} + jZ_{img} \quad (9)$$

where Z_{real} and Z_{img} represent the real and the imaginary parts of the impedance. Based on the

expression of the impedance, the magnitude and phase of the impedance can also be calculated as,

$$|Z| = \sqrt{{Z_{real}}^2 + {Z_{img}}^2} \quad (10)$$

$$\phi = tan^{-1}\left(\frac{Z_{img}}{Z_{real}}\right) \quad (11)$$

It can be shown in Fig. 6 that both the real part and the magnitude of the impedance vary obviously and monotonically with temperatures in the whole frequency range. As for the imaginary part and the phase, their variations with temperature can only be significant under the frequency range between 4 Hz and 365 Hz.

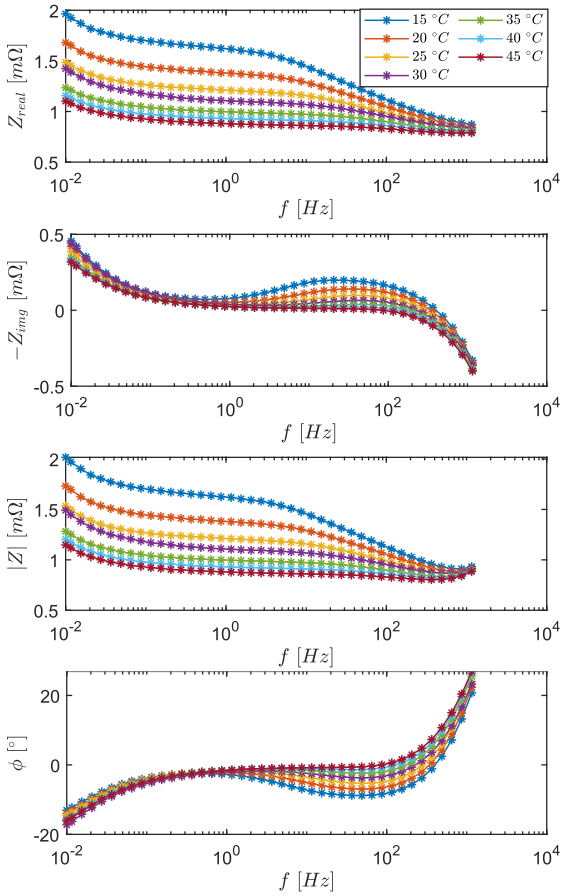

Fig. 6. Impedance parameters at different temperatures when battery SOC is 50%.

Since the variation of the imaginary part and the phase of battery impedance with temperature is not monotonic at a wide frequency, they will not be analyzed in the later part of this paper. As for the real part and the magnitude of the impedance, they are quite close to each other. Owing to the fact that the magnitude of the impedance can be calculated directly from voltage and current measurement, the magnitude of impedance will be used to estimate battery SOT in this paper.

Since the magnitude of battery impedance has a monotonic change with temperature in a wide frequency range, as shown in Fig. 6, any frequency which is suitable for battery operation can be applied. Here, the magnitude of the impedance at 11.5 Hz can be selected for estimation as an example. A 2nd order polynomial is used to model the measured magnitude of impedance and the estimated temperatures, and the results can be shown in Fig. 7. The modeled temperature estimation equation is,

$$\hat{T} = 55.82|Z|^2 - 178.41|Z| + 156.39 \quad (9)$$

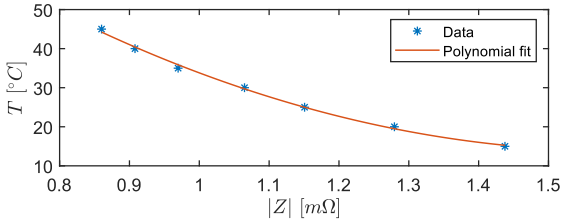

Fig. 7. Temperature estimation results based on 2nd order polynomial.

Table II: Estimation Errors

T_{real} / ℃	$\hat{T}$ / ℃	Estimation Error / ℃
15	15.3	0.3
20	19.5	−0.5
25	24.9	−0.1
30	29.7	−0.3
35	35.9	0.9
40	40.4	0.4
45	44.2	−0.8

The estimation results and errors can be summarized in Table II. The R-square of the modeling results is 0.9972 and the root mean square error (RMSE) is 0.7 ℃, indicating a good interpretation of the impedance-temperature relationship. In real applications, by measuring the real part of impedance at 11.5 Hz online, the battery temperature can be estimated timely.

SOT estimation at varying SOCs

To investigate the effect of SOCs on impedance, the impedance parameters are extracted from battery EIS at different SOCs. Fig. 8 illustrates the Bode plots of the battery EIS at different SOCs at 25 ℃. As shown in Fig. 8, the impedance parameters show insignificant changes to SOCs when battery SOC is higher than 30%. The variation of impedance parameters at the frequency region lower than 10 Hz is more notable than that in the higher frequency region. When battery SOC is below 30%, both the real part and the magnitude of the impedance deviate remarkably from the impedance above 30% SOC, particularly at the frequency region between 0.01 Hz and 10 Hz. It should be noted that when the frequency is higher than 10 Hz, the impedance parameters at different SOCs begin to converge

so that in this region the effect of SOC on impedance parameters becomes smaller.

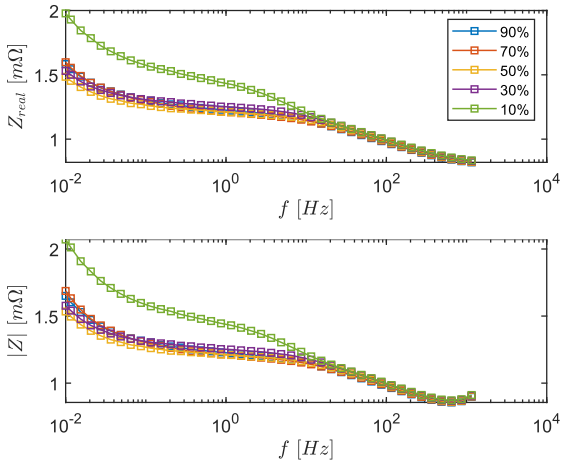

Fig. 8. Impedance parameters at different SOCs when the battery temperature is at 25 ℃.

It can be concluded from Fig. 8 that in some frequency ranges the effect of SOC on impedance parameters cannot be ignored. As a result, the uncertainties of SOC will interfere with the SOT estimation. Therefore, in the SOT estimation loop, the effect of SOC should be eliminated. To this end, an appropriate frequency must be found, under which the impedance parameters are sensitive to temperature change but insensitive to SOC change.

To find the suitable excitation frequency for SOT estimation, the dependency of impedance parameters on battery temperature and SOC at different frequencies should be calculated in advance. Since it is unlikely for the battery to operate in an extremely low SOC range, the electrochemical impedance at 10% is not included in the SOT estimation. The sensitivity of impedance parameters with temperatures and SOCs, as defined in Eq. (3) and Eq. (4), are shown in Fig. 9 and

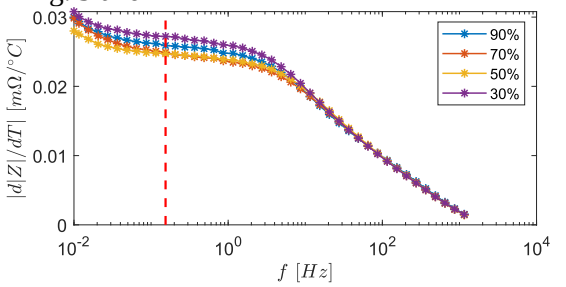

Fig. 9: Absolute sensitivity of impedance parameters to battery temperature at different SOC levels.

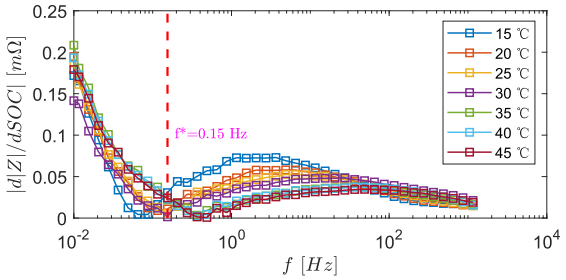

Fig. 10: Absolute sensitivity of impedance parameters to battery SOC at different temperatures.

As can be seen from Fig. 10, the impedance parameters of the battery become less sensitive to SOC when the frequency is from 0.04 Hz to 1 Hz. Under this frequency range, all the impedance parameters still remain high sensitivity to temperature change, as shown in Fig. 9. Therefore, we can choose an excitation frequency from 0.04 Hz to 1 Hz region so that the effect of SOC uncertainties on SOT estimation can be ignored while the impedance parameters remain high sensitivity to temperature change. In our case, we select 0.15 Hz as the excitation frequency and use the magnitude of impedance at 50% SOC to parameterize the impedance-temperature relationship. Likewise, a 2nd order polynomial is used to model this relationship. The fitting results of the impedance-parameter relationship can be shown in Fig. 11(a). The R-square and the RMSE of the model fitting are 0.9934 and 1.1 ℃, respectively, indicating good model parameterization. To further examine the model performance on SOT estimation under different SOCs, the impedance data at 90%, 70%, and 30% SOCs are used for validation. The estimation results are shown in Fig. 11(b), where the estimation error can be summarized in **Table III**.

It can be indicated from Fig. 11(b) and Table III that the SOT estimation under different SOCs is accurate. The RMSEs at 90%, 70%, and 50% SOCs are 1.4 ℃, 1.3 ℃, and 1.3 ℃, respectively. In addition, it can be concluded from Table III that the estimation has higher errors in the high-temperature region, particularly when the temperature is above 40 ℃. This is due to the reason that the change of impedance in the high-temperature region is small so that a small deviation in the impedance input can cause significant estimation error.

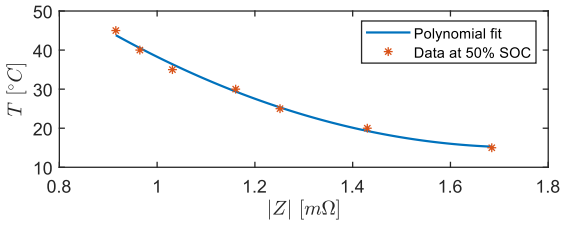

(a)

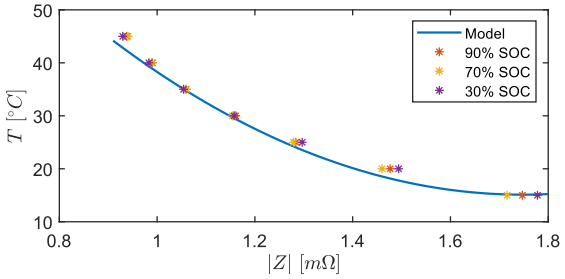

(b)

Fig. 11. Impedance-temperature modeling and the estimation results based on 2nd order polynomial by considering the variation of battery SOC. (a) Modeling results, (b) Estimation using impedance measurement at different SOCs.

Table III: Estimation error under varying SOC.

T_{real} / °C	Error at 90% SOC/ °C	Error at 50% SOC / °C	Error at 30% SOC / °C
15	0.1	0.2	0.2
20	−1.8	−1.5	−2.2
25	−1.0	−0.8	−1.5
30	−0.6	−0.3	−0.5
35	−0.2	−0.3	0.1
40	−1.1	−1.0	−0.7
45	−2.7	−2.9	−2.2

Conclusion

In this paper, we are proposing a novel method for sensorless estimating the battery volume temperature based on electrochemical impedance measurement. Conventionally impedance measurement is only available using EIS technique and expensive measuring instruments which are not practical for online- measurements in an EV. Assuming the battery pack build with Smart Battery technology including the availability of cell-level bypass, the measurement of impedance in ac becomes possible by switching the bypass with a certain frequency and using the data measuring and computation capability available at the cell level. The first challenge addressed is to find the most suitable frequency for impedance measurement and this was found by trying to maximize the sensitivity of impedance to temperature and minimizing the sensitivity to SOC. This resulted in a very low excitation frequency of 0.15 Hz for a realistic prismatic cell of 50 Ah which also reduces the switching losses associated with the measurement. The temperature estimation was verified against laboratory EIS measurement and the RMSE was 0.7 Celsius for the SOC stable case, well inside the normal temperature measurement tolerance by industrial BMS of 1%. This could have a positive impact on the cost of future Smart Battery systems and future work envisages implementation and validation of the real prototype.

References

[1] "EV-Volumes - The Electric Vehicle World Sales Database." https://www.ev-volumes.com/ (accessed Mar. 06, 2023).

[2] X. Hu, F. Feng, K. Liu, L. Zhang, J. Xie, and B. Liu, "State estimation for advanced battery management: Key challenges and future trends," *Renewable and Sustainable Energy Reviews*, vol. 114, p. 109334, Oct. 2019, doi: 10.1016/j.rser.2019.109334.

[3] Y. Zeng, D. Chalise, S. D. Lubner, S. Kaur, and R. S. Prasher, "A review of thermal physics and management inside lithium-ion batteries for high energy density and fast charging," *Energy Storage Mater*, vol. 41, no. May, pp. 264–288, Oct. 2021, doi: 10.1016/j.ensm.2021.06.008.

[4] M.-T. F. Rodrigues *et al.*, "A materials perspective on Li-ion batteries at extreme temperatures," *Nat Energy*, vol. 2, no. 8, pp. 1–14, 2017, doi: 10.1038/nenergy.2017.108.

[5] Y. Che, X. Hu, X. Lin, J. Guo, and R. Teodorescu, "Health prognostics for lithium-ion batteries: mechanisms, methods, and prospects," *Energy Environ Sci*, vol. 16, no. 2, pp. 338–371, 2023, doi: 10.1039/D2EE03019E.

[6] X. Lin, H. E. Perez, J. B. Siegel, and A. G. Stefanopoulou, "Robust estimation of battery system temperature distribution under sparse sensing and uncertainty," *IEEE Transactions on Control Systems Technology*, vol. 28, no. 3. pp. 753–765, 2020. doi: 10.1109/TCST.2019.2892019.

[7] X. Du, J. Meng, J. Peng, Y. Zhang, T. Liu, and R. Teodorescu, "Sensorless Temperature Estimation of Lithium-ion Battery based on Broadband Impedance Measurements," *IEEE Trans Power Electron*, vol. PP, no. c, pp. 1–1, 2022, doi: 10.1109/tpel.2022.3166170.

[8] L. H. J. Raijmakers, D. L. Danilov, J. P. M. Van Lammeren, M. J. G. Lammers, and P. H. L. Notten, "Sensorless battery temperature measurements based on electrochemical impedance spectroscopy," *J Power Sources*,

vol. 247, pp. 539–544, 2014, doi: 10.1016/j.jpowsour.2013.09.005.
[9] R. Teodorescu, X. Sui, S. B. Vilsen, P. Bharadwaj, A. Kulkarni, and D.-I. Stroe, “Smart Battery Technology for Lifetime Improvement,” *Batteries*, vol. 8, no. 10, p. 169, Oct. 2022, doi: 10.3390/batteries8100169.
[10] Abhijit Kulkarni, Hoda Sorouri, Yusheng Zheng, Xin Sui, Arman Oshnoei, and Nicolai André Weinreich, “Li-ion Battery Digital Twin Based on Online Impedance Estimation,” in *CPE-POWERENG 2023*,